Chapter 13

Extended Gate Field-Effect Transistor Biosensors for Point-Of-Care Testing of Uric Acid

Weihua Guan and Mark A. Reed

Abstract

An enzyme-free redox potential sensor using off-chip extended-gate field effect transistor (EGFET) with a ferrocenyl-alkanethiol modified gold electrode has been used to quantify uric acid concentration in human serum and urine. Hexacyanoferrate (II) and (III) ions are used as redox reagent. The potentiometric sensor measures the interface potential on the ferrocene immobilized gold electrode, which is modulated by the redox reaction between uric acid and hexacyanoferrate ions. The device shows a near Nernstian response to uric acid and is highly specific to uric acid in human serum and urine. The interference that comes from glucose, bilirubin, ascorbic acid, and hemoglobin is negligible in the normal concentration range of these interferents. The sensor also exhibits excellent long term reliability and is regenerative. This extended gate field effect transistor based sensor is promising for point-of-care detection of uric acid due to the small size, low cost, and low sample volume consumption.

Key words Extended gate FET, Redox, Enzyme-free, Uric acid, Potentiometric sensor, Ferrocenyl-alkanethiol

1 Introduction

As the primary end product of purine metabolism, high concentrations of uric acid (UA) in the human body can be used as a biomarker and have been linked to many diseases such as gout, Lesch–Nyhan syndrome, cardiovascular disease, type 2 diabetes, metabolic syndrome, and kidney stones [1]. Lower serum values of uric acid have been associated with multiple sclerosis [2]. It is clinically important to monitor the concentration of UA in biological fluids for the early detection of these conditions and for patient diagnosis. To that end, a simple, reliable, and inexpensive detection system is highly desirable and would be especially useful for point-of-care testing.

Current in vitro quantification of UA concentration usually involves the redox properties of UA. A first approach for quantification of UA uses reduction of phosphotungstate to tungsten blue

Ben Prickril and Avraham Rasooly (eds.), *Biosensors and Biodetection: Methods and Protocols, Volume 2: Electrochemical, Bioelectronic, Piezoelectric, Cellular and Molecular Biosensors*, Methods in Molecular Biology, vol. 1572,
DOI 10.1007/978-1-4939-6911-1_13,

in an alkaline solution (pH 9–10), which is measured photometrically [3]. The method is, however, subject to interference from drugs and reducing substances other than UA. A second approach, which is the current clinical method of UA analysis, adopts an enzymatic method to specifically detect UA. Uricase is used to catalyze the oxidation of UA by oxygen into allantoin, carbon dioxide, and hydrogen peroxide [4–6]. Besides the redox method, other approaches for UA analysis includes high performance liquid chromatography (HPLC) on reversed phase columns along with detection by either UV absorbance [7] or mass spectrometry [8]. These methods involve complex sample and reagent preparation steps, and require bulky and expensive spectroscopic equipment to quantify the concentration. These drawbacks make them unsuitable to be used for point-of-care testing.

Electrochemical techniques for UA detection have attracted much attention due to their fast response, simple testing procedure, cheap instrumentation, and high selectivity and sensitivity [9]. Electrochemical UA detection is currently performed using an amperometric method [10]. However, the sensitivity of amperometry depends on the electrode area and it is therefore difficult to decrease the sample volume. Thus a potentiometric sensor is preferred since signal intensity is independent of detection volume. In general, electrochemical sensor approaches can be divided into enzymatic and nonenzymatic. Enzymatic sensors use enzymes to convert the analyte into a product that is sensor-detectable. A well-known example of this is the amperometric enzyme glucose sensor developed in 1973 [11], in which the anodic production of hydrogen peroxide was analyzed instead of the highly variable oxygen reduction current. Non-enzymatic (or enzymeless) sensors mostly rely on the chemical activity of transition metal centers and have garnered significant interest due to their capacity to achieve continuous monitoring, high stability compared to traditional enzymatic sensors, and ease of fabrication. Enzymatic approaches suffer from an enzyme degradation problem and are hard to store for extended periods; therefore research has been extensively directed towards nonenzymatic sensors using novel materials that often have unique micro- or nano-structures. Since UA can be easily oxidized in aqueous solution, the nonenzymatic approach is both feasible and favorable. However, interference resulting from ascorbic acid must be minimized [12]. Recent approaches adopt chemical modifications on the electrodes to enhance the selectivity [9, 13–15].

In this work, we report an enzyme-free potentiometric UA sensor based on an off-chip extended-gate field effect transistor (EGFET) with a ferrocenyl-alkanethiol modified gold electrode. The extended gate functions as the sensing interface, whereas the field effect transistor functions as an in situ trans-impedance

amplifier that converts a small potentiometric voltage into a readable signal. By leveraging the advantages of microelectronic integration, the EGFET can be made very compact. The hexacyanoferrate (II) and (III) ions are used as redox reagent. This potentiometric sensor measures the interface potential on the ferrocene immobilized gold electrode, which can be modulated by the redox reaction between UA and hexacyanoferrate ions. The EGFET based sensor has shown high selectivity, sensitivity, reliability, and accuracy to UA detection in human serum and urine. Its small size, low cost, low sample volume consumption (<10 μL), and easy operation make this device a potential point-of-care UA testing tool.

2 Materials

2.1 Chemicals

1. 11-(ferrocenyl)undecanethiol (Catalog No. 738905, Sigma-Aldrich, St. Louis, MO).
2. Ethanol (Catalog No. 459844, Sigma-Aldrich, St. Louis, MO).
3. 1 M nitric acid (Catalog No. 35315, Sigma-Aldrich, St. Louis, MO).
4. Sodium sulfate (Catalog No. 239313, Sigma-Aldrich, St. Louis, MO).
5. Potassium chloride (Catalog No. 746436, Sigma-Aldrich, St. Louis, MO).
6. Potassium hexacyanoferrate(II) trihydrate (Catalog No. P3289, Sigma-Aldrich, St. Louis, MO).
7. Potassium hexacyanoferrate(III) (Catalog No. 244023, , Sigma-Aldrich, St. Louis, MO).
8. pH standard solution (Catalog No. 0029-04, 0031-04, and 0032-04, Brand-Nu Laboratories, USA).
9. Uric acid (Catalog No. 02103215, MP Biomedicals, USA).
10. Human serum from male AB clotted whole blood and sterile-filtered (Catalog No. H6914, St. Louis, MO).
11. Glucose (Catalog No. 410955000, Acros Organics, USA).
12. Ascorbic acid (Catalog No. RDCA0750-100B1, Ricca Chemical, USA).
13. Bilirubin (Catalog No. 230225000, Acros Organics, USA).
14. Hemoglobin (Catalog No. H7506-STD, Pointe Scientific, USA).
15. Phosphate buffered saline (Catalog No. P4417, St. Louis, MO).

2.2 Electronics

1. N-channel enhancement mode MOSFETs (ALD110800, Advanced Linear Devices).
2. Custom built printed circuit board (PCB), accompanying signal amplification and data acquisition interface for personal computers (Dell PC).
3. Ag/AgCl electrodes (Catalog No. 69-0053, Warner Instruments).
4. Ceramic chip carrier (Global Chip Materials).
5. Linear voltage regulator chips are used in the integrated PCB as the power source (9 V).
6. All other components (resistors, capacitors, op-amps, BNC connectors, etc.) are from Newark.

2.3 Software

1. CadSoft EAGLE PCB design software for designing custom-built printed circuit board, and the designed board can be manufactured by commercial vendors such as OSH Park.
2. Labview program is used for data acquisition.
3. MATLAB for data analysis.

2.4 Facilities

1. The fabrication of the extended gate chip is performed in a class 1000 cleanroom.
2. EVG620 is used for lithography.
3. Metal evaporation is performed with e-beam evaporation equipment.
4. Chromium mask is prepared using Heidelberg direct laser writing (this can also be done by using commercial vendors).
5. An in-house high precision wafer dicing at Yale cleanroom is used for dicing the wafer.

3 Methods

3.1 Sensing Principles

Figure 1 shows the uric acid sensing principle using EGFET.

For the ferrocene-modified gold electrode, the interfacial potential (E) is determined by the redox state of the ferrocene compounds on the gold electrode and is given by the Nernstian equation,

$$E = E_0 - \frac{RT}{F} \ln \frac{[\mathrm{Fc}]}{[\mathrm{Fc}^+]} \tag{1}$$

where E_0 is the standard electrode potential, R is the gas constant, T is the absolute temperature, and F is the Faraday constant. [Fc] and [Fc^+] are the ferrocene and ferrocenium ion concentrations, respectively.

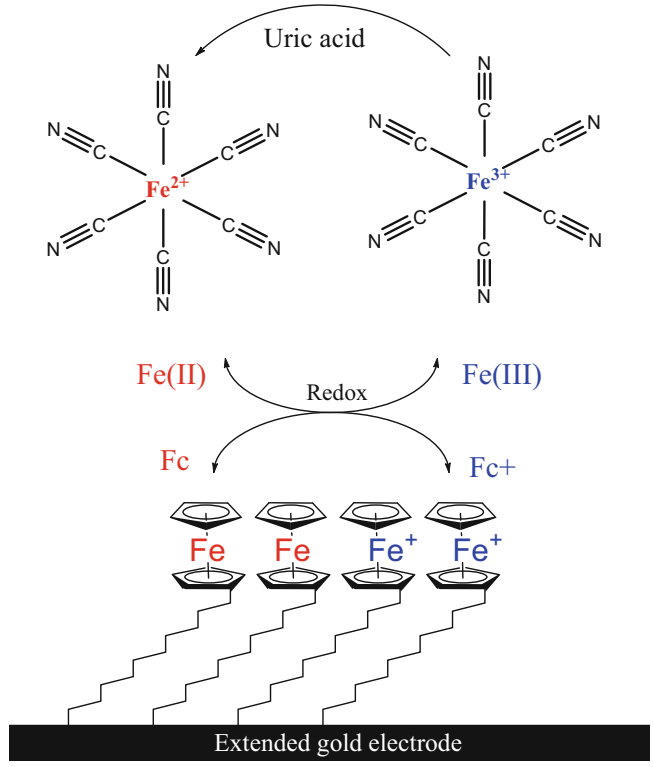

Fig. 1 Uric acid sensing principle. The change in the ratio of hexacyanoferrate ions (Fe(II) and Fe(III)) induced through the oxidation of uric acid can be detected by the ferrocenyl-alkanethiol modified-FET sensor as the interfacial potential. Reproduced from Biosensors and Bioelectronics 2014 with permission from Elsevier [16]

Due to their high reactivity with ferrocene compounds on the gold electrodes, hexacyanoferrate ions were widely used as the redox compound, given by the following reaction:

$$\mathrm{Fc} + \left[\mathrm{Fe(CN)_6}\right]^{3-} \rightleftarrows \mathrm{Fc^+} + \left[\mathrm{Fe(CN)_6}\right]^{4-} \tag{2}$$

where $[Fe(CN)_6]^{3-}$ and $[Fe(CN)_6]^{4-}$ is hexacyanoferrate(III) and hexacyanoferrate(II), respectively. At equilibrium, the concentration relationship among the four components in Eq. 2 is described by using thermodynamic equilibrium constant (K),

$$\frac{[\mathrm{Fc}]}{[\mathrm{Fc^+}]} = K\frac{[\mathrm{Fe(II)}]}{[\mathrm{Fe(III)}]} \tag{3}$$

where [Fe(II)] and [Fe(III)] denotes the concentration of $[Fe(CN)_6]^{4-}$ and $[Fe(CN)_6]^{3-}$, respectively. By substituting Eq. 3 into Eq. 1, the interfacial potential can be written as,

$$E = E_0 - \frac{RT}{F}\ln\frac{[\mathrm{Fe(II)}]}{[\mathrm{Fe(III)}]} \tag{4}$$

Eq. 4 shows that the ratio of hexacyanoferrate (II) concentration to hexacyanoferrate (III) concentration can be determined by measuring the interfacial potential of the ferrocene immobilized gold electrode. In theory, the sensitivity of the interfacial potential should be −59 mV/decade at room temperature.

Morin et al. described an acid ferric reduction procedure for specifically determining serum uric acid with colorimetric readout [17], whereby each mole of UA reduces N moles of ferric ion (N~4, depending on the pH value and temperature). As a result, by introducing V μL of UA with a concentration [UA] into V μL of hexacyanoferrate(III) solution with concentration $[\mathrm{Fe(III)}]_0$, the concentrations of hexacyanoferrate (III) and hexacyanoferrate (II) after reaction is thus given by,

$$\begin{aligned}[\mathrm{Fe(III)}] &= \frac{[\mathrm{Fe(III)}]_0 - \mathrm{N[UA]}}{2} \\ [\mathrm{Fe(II)}] &= \frac{\mathrm{N[UA]}}{2}\end{aligned} \tag{5}$$

Therefore, by combining Eqs. 4 and 5, the interfacial potential can be rewritten as,

$$\mathrm{E} = \mathrm{E}_0 - \frac{\mathrm{RT}}{\mathrm{F}}\ln\frac{\mathrm{N[UA]}}{[\mathrm{Fe(III)}]_0 - \mathrm{N[UA]}} \tag{6}$$

Under the condition where the initial hexacyanoferrate(III) concentration is much excessive to oxidize the UA, i.e., $[\mathrm{Fe(III)}]_0 \gg \mathrm{N[UA]}$, Eq. 6 can be reduced into the form of,

$$E = E_0^* - \frac{RT}{F}\ln[\mathrm{UA}] \tag{7}$$

where $E_0^* = E_0 + \frac{RT}{F}\ln\frac{[\mathrm{Fe(III)}]_0}{\mathrm{N}}$ is a constant for one specific measurement situation. It is noteworthy that a According to Eq. 7, UA concentration can be determined by measuring the interfacial potential of the ferrocenyl-alkanethiol modified gold electrode, and the theoretical sensitivity of this detection is about −59 mV/pUA.

3.2 Extended Gate FET Fabrication

1. The off-chip EGFET UA sensor consists of two independent parts (Fig. 2): a disposable front-end sensing chip made of multiple interdigitated gold electrodes and a reusable back-end FET to detect the interfacial potential on the gold electrode.
2. The front-end gold electrode (80 nm Au on top of 20 nm of an adhesive Cr layer) are manufactured sequentially by

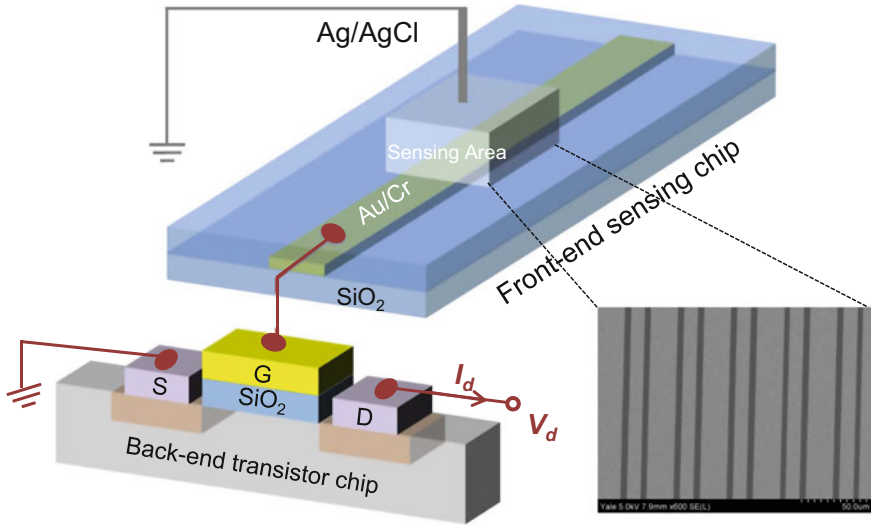

Fig. 2 Schematic of the off-chip extended gate field effect transistor sensor configuration. It consists of two independent parts: a disposable front-end sensing chip and a reusable back-end detection transistor. A Ag/AgCl reference electrode is used to set a stable reference potential. S, D, G: Source/Drain/Gate terminal for the ALD110800 MOSFET. V_d is the voltage applied to the drain terminal. I_d is the drain terminal current. The sensing area is the liquid chamber for the reaction. Reproduced from Biosensors and Bioelectronics 2014 with permission from Elsevier [16]

photolithography, e-beam metal evaporation, and a lift-off process (http://www.microchemicals.com/technical_information/lift_off_photoresist.pdf) on a 4 in Si wafer with 3-μm-thick SiO_2 as an isolating layer. The whole wafer is protected by another layer of SiO_2 layer except the sensing area (reaction chamber) and the bonding pads.

3. Each chip is diced with dicing saw in-house (Yale Engineering Cleanroom). Each chip is around 20 mm × 17 mm.

3.3 Functionalization of Gold Electrodes

1. Solid 11-(Ferrocenyl)undecanethiol is dissolved in ethanol to form a 1 mM 11-(Ferrocenyl)undecanethiol solution.
2. The extended gold electrode chips (patterned gold electrodes on silicon oxide substrate) are dipped into 1 M nitric acid for 15 s and rinsed immediately with DI water.
3. The washed extended gold electrode chips are then immersed and kept in the 1 mM 11-(Ferrocenyl)undecanethiol solution at room temperature for 24 h to fully functionalize the gold electrodes.
4. After functionalization, the chips are rinsed with pure ethanol and DI water before storing them in 100 mM sodium sulfate solution at room temperature. Once stored, the surface functionalization is stable for over 1 year.

3.4 Electrical Setup

1. The front-end sensing chip is wire-bonded into a ceramic chip carrier using West Bond 7440E—ultrasonic insulated wire bonder.
2. The chip carrier is the plugged onto a custom-built printed circuit board (PCB), accompanying signal amplification and data acquisition interface for personal computers (Fig. 3).
3. Ag/AgCl electrode is used as reference electrode and is held at a constant potential of 0 V during all tests. The modular configuration of a separate front-end sensing chip and a back-end transistor chip has clear advantages in terms of cost and disposability (plug-and-measure).
4. Ag/AgCl electrode is prepared in house by supplying 2 V to the silver wire against a Pt wire in 1 M KCl solution for 20 min.
5. ALD110800 is configured by connecting the gate terminal to the extended gate chip. The source and drain of the FET is biased at 0.1 V (Fig. 4).

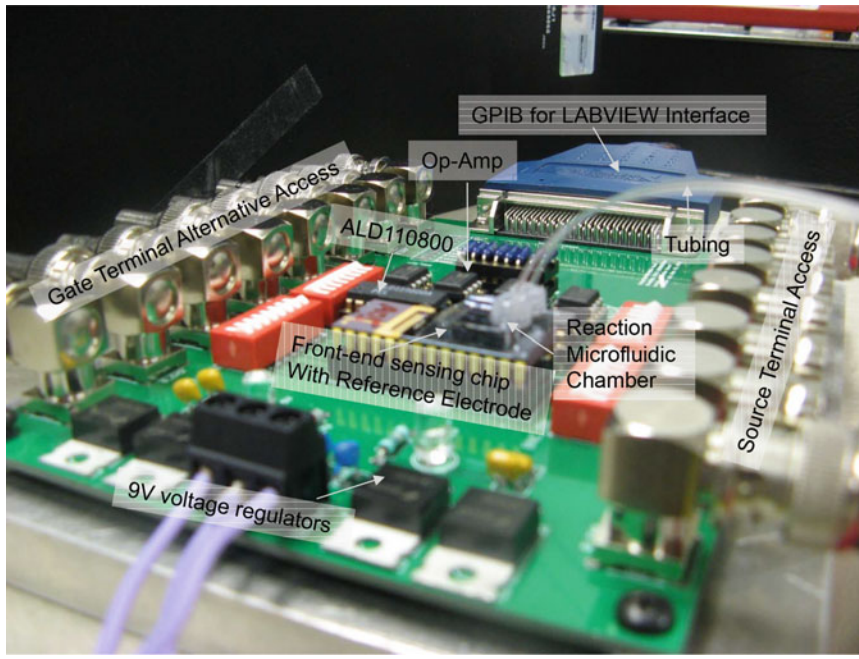

Fig. 3 Photograph of electrical testing setup. The labels shows the physical location of components shown in Fig. 2. The ALD10880 is used as the backend transistor chip and the ceramic carrier holds the disposable front-end sensing chip and the Ag/AgCl electrode. The system is powered by 9 V voltage regulators. The gate terminal alternative access provides the ports for system testing while source terminal access provides the ports for applying source voltages. Liquid is pumped into the system using a syringe pump, though the liquid can also be dispensed with a pipette

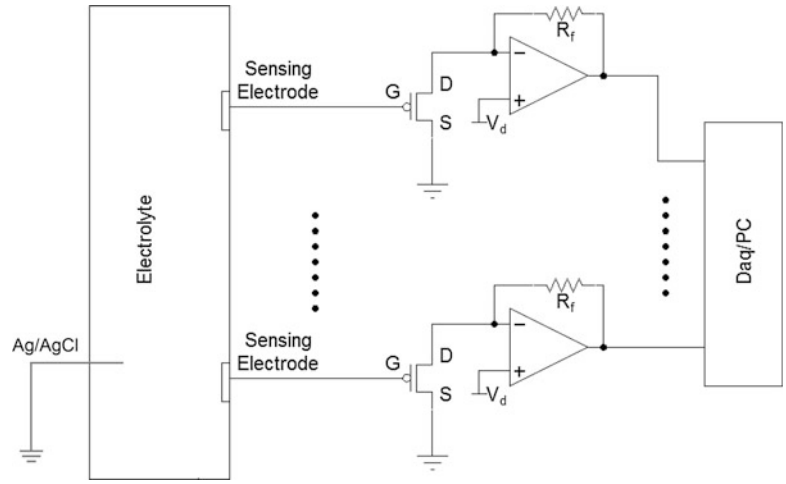

Fig. 4 The schematic of the circuit diagram for constructing the PCB board used in Fig. 3

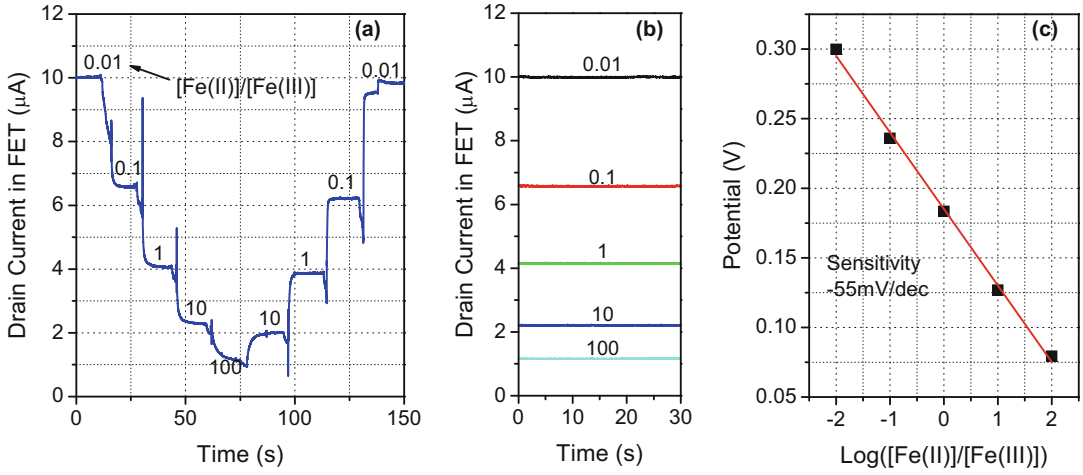

Fig. 5 The device response to different [Fe(II)]/[Fe(III)] ratios. (**a**) Time course of the source–drain current when the device is subject to a continuous set of different [Fe(II)]/[Fe(III)] ratios. The total concentration of the mixed hexacyanoferrate solution is 10 mM, (**b**) A separate time course for each individual [Fe(II)]/[Fe(III)] ratio at 10 mM concentration. Each different line represents a different [Fe(II)]/[Fe(III)] ratio (0.01–100), (**c**) The extracted interface potential as a function of the log ratio of [Fe(II)]/[Fe(III)] for (**a**) and (**b**), the slope of which is determined to be -55.01 ± 1.52 mV/decade. Reproduced from Biosensors and Bioelectronics 2014 with permission from Elsevier [16]

3.5 Device Characterization with [Fe(II)]/[Fe(III)]

1. Different concentration ratio of hexacyanoferrate (II) to hexacyanoferrate (III), ranging from 10^{-2} to 10^{2} (prepared in 1× phosphate buffered saline (PBS buffer) solution) is used to characterize the functionality of the device.
2. Figure 5a exhibits the real time response to different [Fe(II)]/[Fe(III)] values. Figure 5b shows the separate time course for

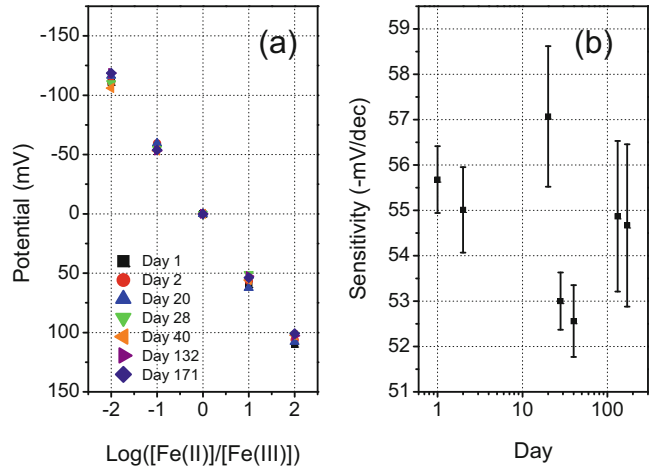

Fig. 6 (**a**) Long term stability of the device response to different [Fe(II)]/[Fe(III)] values. (**b**) The interfacial potential values in are normalized at [Fe(II)]/[Fe(III)] = 1 to be 0 mV for different days. Reproduced from Biosensors and Bioelectronics 2014 with permission from Elsevier [16]

each [Fe(II)]/[Fe(III)] value. The extracted interfacial potential (Fig. 5c) exhibits a near Nernstian response (Eq. 4) to the ratio of [Fe(II)]/[Fe(III)], with a slope of around −55 mV/decade.

3. Device response to different salt concentration values are characterized. Using 10 mM of 1:1 mixed Fe(II)/Fe(III) solutions, the 11-(ferrocenyl)undecanethiol modified EGFET sensor showed no response to the added KCl salts from 10 mM to 1 M (*see* **Note 1**).
4. In addition, device response to different pH values is characterized. It showed no response to pH values ranging from 4 to 12 (*see* **Note 2**).
5. To ensure the long term stability of the 11-(ferrocenyl) undecanethiol modified gold electrode, we monitored the same device's response to [Fe(II)]/[Fe(III)] values over time. As shown in Fig. 6, the device response to [Fe(II)]/[Fe(III)] did not degrade over a time course of 6 months.

3.6 Device Characterization with Clean UA

1. After confirming the device response to [Fe(II)]/[Fe(III)] values, we tested the device response to clean UA. Figure 7a shows the real time device response when dropping 5 μL of freshly prepared UA of different concentrations into 5 μL of 10 mM hexacyanoferrate (III) solutions. The end point evaluation of the complete reaction between UA and Fe(III) can be done after about 5 min (which is the assay time).
2. The relationship between the extracted interfacial potential and the UA concentration is shown in Fig. 7b. The interfacial

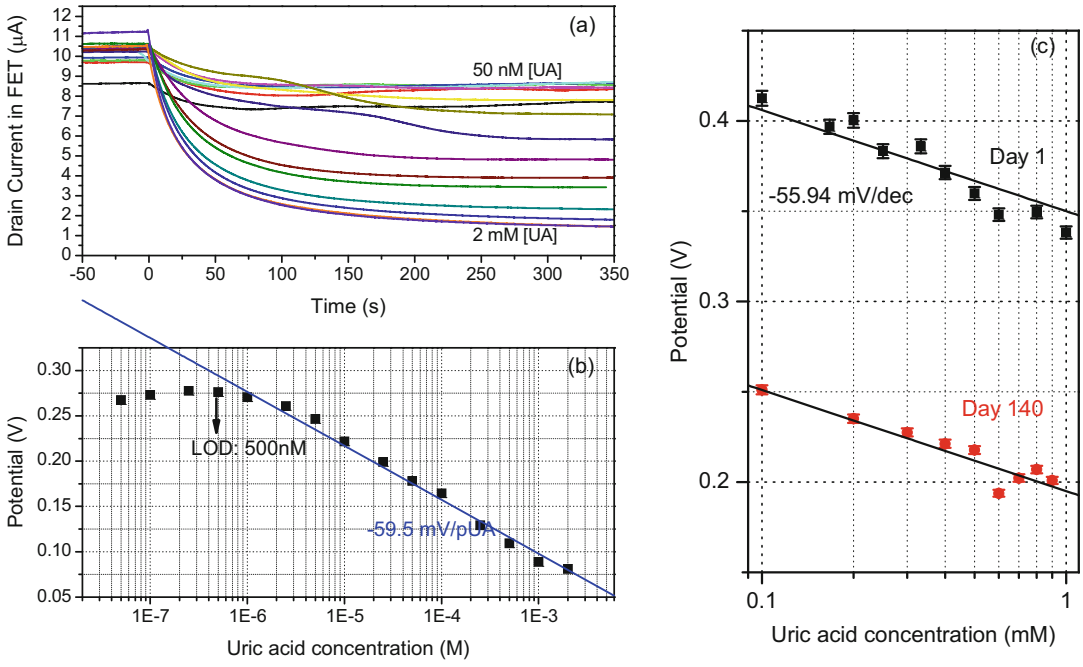

Fig. 7 Device response to artificially prepared UA in 10 mM hexacyanoferrate (III) solutions. (**a**) Time course of the source–drain current for different UA concentrations. Time $t = 0$ is when the UA is dropped into the hexacyanoferrate (III) solutions, (**b**) The extracted end point interfacial potential for different UA concentrations shown in (**a**), (**c**) Long term response to artificially prepared UA with the same device. The sensitivity of the device shows a similar value of −55.94 mV/pUA over a period of 140 days. The coefficient of variation (CV) of the error bar is 1%. The vertical shift in the potential value is intentionally added for easy visualization. Reproduced from Biosensors and Bioelectronics 2014 with permission from Elsevier [16]

potential has a good linearity to the logarithm of UA concentration from 1 μM to 1 mM (with a slope around −59.5 mV/pUA). As a result, the device has a linear dynamic range over three orders of magnitude. The response saturates when the UA concentration is less than 500 nM and the detection limit of this EGFET sensor is therefore determined to be around 500 nM.

3. To further test the reliability of the device response to UA, we carried out two measurements. The first test is the device to device variation. A total of six different devices are tested using the same set of reagents and the response for each is almost the same as that illustrated in Fig. 7a, b. The second test is the long term stability of the device response to UA. Figure 7c shows the same device's response to UA of different concentrations for a time period of 140 days. No device response deterioration is observed over this time period.

3.7 Device Response to Biological Samples

1. Test the device response to serially diluted biological solutions. Figure 8a shows the end point interfacial potential as a function of dilution ratio when adding 5 μL serially diluted human

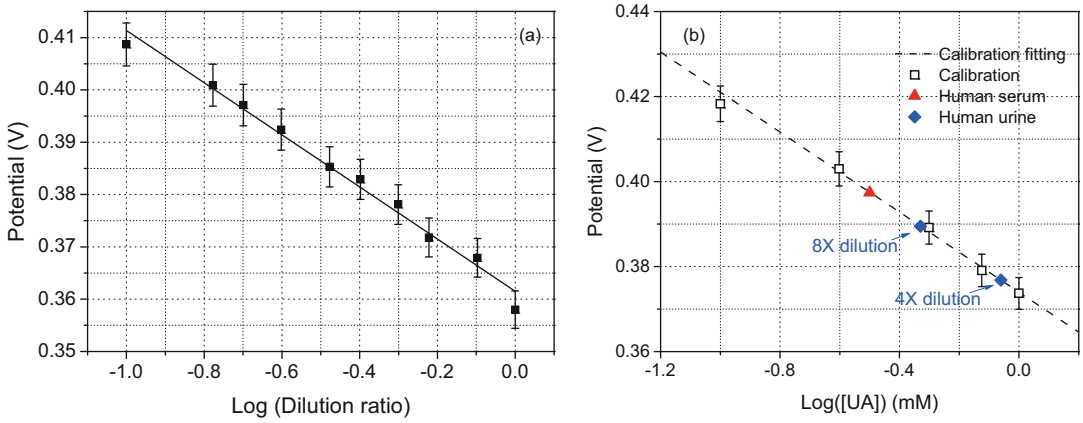

Fig. 8 The device response to biological samples. (**a**) Device response to serially diluted human serum solutions. The sensitivity in this specific device is determined to be -49.8 ± 2.01 mV/decade. The coefficient of variation of the error bar is 1%. (**b**) Quantitative detection of uric acid in biological samples. The calibration curve is generated by the known UA concentration (*empty squares*), which is used to determine the unknown uric acid concentration in the biological samples (*filled triangle and diamond*). The coefficient of variation of the error bar is 1%. Reproduced from Biosensors and Bioelectronics 2014 with permission from Elsevier [16]

serum into 5 μL of 1 mM hexacyanoferrate (III) solutions. The interfacial potential shows a good linearity to the logarithm of dilution ratios. This confirms that the device can work with the biological samples containing complex bio-components.

2. Test the UA concentration in biological samples with an assay type setup. The device response to different concentrations of artificially prepared UA solutions is tested to generate a calibration curve (empty squares in Fig. 8b). The calibration curve is generated using 5 μL of UA with a concentration range of 0.1–1 mM in 5 μL of 10 mM hexacyanoferrate (III) solution. The calibration curve can be fitted by,

$$E = -0.04709\log[\mathrm{UA}] + 0.37396 \quad (8)$$

where [UA] is in the unit of mM. Eq. 8 correlates the [UA] with the interfacial potential in this specific test. The end point interfacial potential is also evaluated for biological samples (filled symbols in Fig. 8b), the uric acid concentration of which is then derived using Eq. 8.

3.8 Interference Test

1. In biological samples such as human serum and urine, common interferences to UA detection are glucose, ascorbic acid, bilirubin, and hemoglobin [17, 18]. We tested the device response to these interferents at a constant UA concentration (500 μM) to study the selectivity of the potentiometric uric acid sensor in the present work (Fig. 9) (*see* **Notes 3** and **4**).
2. Figure 9a shows the glucose interference. Upon adding glucose with a concentration from 1 to 20 mM to the UA

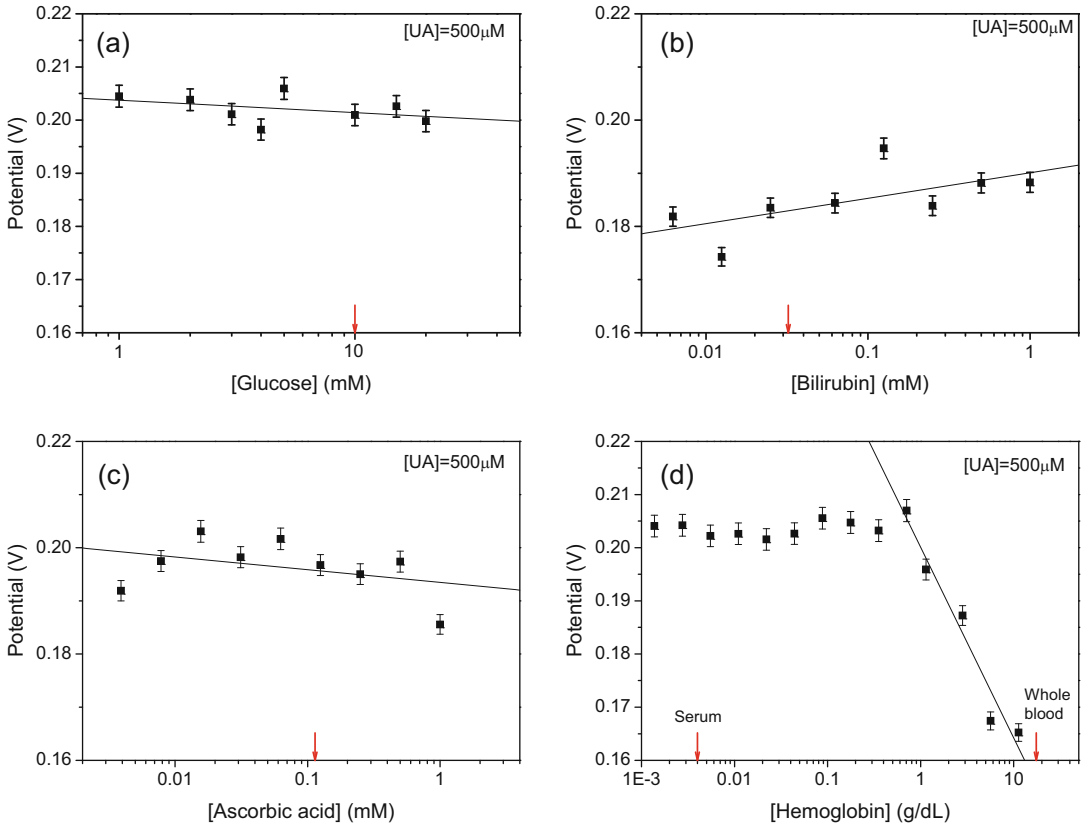

Fig. 9 Interference of (**a**) glucose, (**b**) bilirubin, (**c**) ascorbic acid, and (**d**) hemoglobin, when dropping interferents with various concentrations into the 500 μM UA solution. The red arrows indicate the reference level of the normal concentration. The slope for each fitted curve is (**a**) $-(2.34 \pm 2.16)$ mV/decade, (**b**) 4.79 ± 2.39 mV/decade, (**c**) $-(2.4 \pm 2.21)$ mV/decade, and (**d**) $-(35.89 \pm 4.49)$ mV/decade. The coefficient of variation of the error bar is 1%. Reproduced from Biosensors and Bioelectronics 2014 with permission from Elsevier [16]

solution, the potential signal barely changed. The sensitivity to the glucose is around $-(2.34 \pm 2.16)$ mV/decade. The presence of glucose in the concentration up to 20 mM has no influence on the sensor's response towards UA.

3. Figure 9b shows the bilirubin interference results. Upon adding bilirubin with a concentration from 6.25 μM to 1 mM to the UA solution, the sensitivity to the bilirubin is around 4.79 ± 2.39 mV/decade and it has very little influence on UA detection.
4. Figure 9c shows the ascorbic acid interference. The sensitivity to the ascorbic acid (from 3.9 μM to 1 mM) is around $-(2.4 \pm 2.21)$ mV/decade. The EGFET sensor thus shows a negligible response to ascorbic acid, which is a major problem in many other electrochemical UA sensors [10, 18].

5. Figure 9d shows the hemoglobin interference. Hemoglobin is the iron-containing oxygen-transport metalloprotein in the red blood cells. As shown in Fig. 9d, the device response to the hemoglobin remains unchanged upon adding hemoglobin with a concentration from 44 to 706 mg/dL. However, the device shows a sensitivity of around $-(35.89 \pm 4.49)$ mV/decade to hemoglobin if the concentration is higher than 706 mg/dL. The interference from hemoglobin is mainly due to the fact that the heme group consists of an iron (Fe) ion which is in the ferrous state to support oxygen and other gases' binding and transport. Since the EGFET sensor for UA detection proposed here is based on the [Fe(II)]/[Fe(III)], additional added ferrous or ferric ions will interference the results.

4 Notes

1. Very acidic conditions (pH $<$ 4) should be avoided in all experiments since highly toxic hydrogen cyanide gas may be evolved ($6H^+ + [Fe(CN)_6]^{3-} \rightarrow 6HCN + Fe^{3+}$). 1× PBS is recommended as high-capacity buffer solution to ensure the pH value is around 7 for safety reasons.
2. The sensitivity of the device is hexacyanoferrate concentration dependent. With decreasing hexacyanoferrate concentration the device sensitivity to the [Fe(II)]/[Fe(III)] ratio is decreased. Hexacyanoferrate solution with a concentration of either 1 mM or 10 mM is adopted as the recommended working concentration.
3. For accurate results hemoglobin concentration should be minimized to less than 1 g/dL from a biological sample before using the EGFET uric acid sensor. Normal hemoglobin concentration is around 1–4 mg/dL in serum and is almost nonexistant in urine. The EGFET uric acid sensor can be reliably used for human serum and urine.
4. Uric acid sample should be tested immediately since it is subject to environmental oxidation, resulting in errors. Highly concentrated uric acid sample should be diluted four- to ten-fold so that the UA concentration in the sample remains within the calibration range (0.1–1 mM).

Acknowledgments

W.G. acknowledges the financial support from Howard Hughes Medical Institute International Student Research Fellowship and Pennsylvania State University. The work was supported in part by

the Defense Threat Reduction Agency under grants HDTRA1-10-1-0037 and HDTRA-1-12-1-0042, and by the U. S. Army Research Laboratory and the U. S. Army Research Office under contract/grant number MURI W911NF-11-1-0024.

References

1. Lakshmi D, Whitcombe MJ, Davis F, Sharma PS, Prasad BB (2011) Electrochemical detection of uric acid in mixed and clinical samples: a review. Electroanalysis 23(2):305–320
2. Spitsin S, Koprowski H (2008) Role of uric acid in multiple sclerosis. In: Advances in multiple sclerosis and experimental demyelinating diseases, vol 318. Springer, Berlin, pp 325–342
3. Folin O, Macallum AB (1912) New method for the (colorimetric) determination of uric acid in urine. J Biol Chem 13(3):363–369
4. Sanders GTB, Pasman AJ, Hoek FJ (1980) Determination of uric-acid with uricase and peroxidase. Clin Chim Acta 101 (2–3):299–303
5. Zhao YS, Yang XY, Lu W, Liao H, Liao F (2009) Uricase based methods for determination of uric acid in serum. Mikrochim Acta 164 (1–2):1–6
6. Ali SMU et al (2011) Selective potentiometric determination of uric acid with uricase immobilized on ZnO nanowires. Sens Actuators B Chem 152(2):241–247
7. Sakuma R, Nishina T, Kitamura M (1987) Deproteinizing methods evaluated for determination of uric-acid in serum by reversed-phase liquid-chromatography with ultraviolet detection. Clin Chem 33(8):1427–1430
8. Lim CK, Pryde DE, Lawson AM (1978) Specific Method for determining uric-acid in serum using high-performance liquid-chromatography and gas chromatography-mass spectrometry. J Chromatogr 149:711–720
9. Xue Y et al (2011) The comparison of different gold nanoparticles/graphene nanosheets hybrid nanocomposites in electrochemical performance and the construction of a sensitive uric acid electrochemical sensor with novel hybrid nanocomposites. Biosens Bioelectron 29(1):102–108
10. Chen JC et al (2005) A disposable single-use electrochemical sensor for the detection of uric acid in human whole blood. Sens Actuators B Chem 110(2):364–369
11. Guilbault GG, Lubrano GJ (1973) An enzyme electrode for the amperometric determination of glucose. Anal Chim Acta 64(3):439–455
12. Adams RE, Betso SR, Carr PW (1976) Electrochemical Ph-stat and controlled current coulometric acid-base analyzer. Anal Chem 48 (13):1989–1996
13. Raj CR, Ohsaka T (2003) Voltammetric detection of uric acid in the presence of ascorbic acid at a gold electrode modified with a self-assembled monolayer of heteroaromatic thiol. J Electroanal Chem 540:69–77
14. Zen JM, Chen YJ, Hsu CT, Ting YS (1997) Poly(4-vinylpyridine)-coated chemically modified electrode for the detection of uric acid in the presence of a high concentration of ascorbic acid. Electroanalysis 9(13):1009–1013
15. Toghill KE, Xiao L, Phillips MA, Compton RG (2010) The non-enzymatic determination of glucose using an electrolytically fabricated nickel microparticle modified boron-doped diamond electrode or nickel foil electrode. Sens Actuators B Chem 147(2):642–652
16. Guan W, Duan X, Reed MA (2014) Highly specific and sensitive non-enzymatic determination of uric acid in serum and urine by extended gate field effect transistor sensors. Biosens Bioelectron 51:225–231
17. Morin LG (1974) Determination of serum urate by direct acid Fe3+ reduction or by absorbance change (at 293 nm) on oxidation of urate with alkaline ferricyanide. Clin Chem 20 (1):51–56
18. Dubois H, Delvoux B, Ehrhardt V, Greiling H (1989) An enzymic assay for uric-acid in serum and urine compared with HPLC. J Clin Chem Clin Biochem 27(3):151–156